Live Streaming of a Single Cell's Life over a Local pH-Monitoring Nanowire Waveguide

Moon-Jung Yong, Byunghwa Kang, Un Yang, Seung Soo Oh,* and Jung Ho Je*

Cite This: Nano Lett. 2022, 22, 6375–6382

Read Online

ACCESS | Metrics & More | Article Recommendations | SI Supporting Information

ABSTRACT: Spatiotemporal pH monitoring of single living cells across rigid cell and organelle membranes has been challenging, despite its significance in understanding cellular heterogeneity. Here, we developed a mechanically robust yet tolerably thin nanowire waveguide that enables in situ monitoring of pH dynamics at desired cellular compartments via direct optical communication. By chemically labeling fluorescein at one end of a poly(vinylbenzyl azide) nanowire, we continuously monitored pH variations of different compartments inside a living cell, successfully observing organelle-exclusive pH homeostasis and stimuli-selective pH regulations. Importantly, it was demonstrated for the first time that, during the mammalian cell cycle, the nucleus displays pH homeostasis in interphase but a tidal pH curve in the mitotic phase, implying the existence of independent pH-regulating activities by the nuclear envelope. The rapid and accurate local pH-reporting capability of our nanowire waveguide would be highly valuable for investigating cellular behaviors under diverse biological situations in living cells.

KEYWORDS: nanowire waveguide, nanosensor, single living cell, intracellular pH monitoring, optical analysis
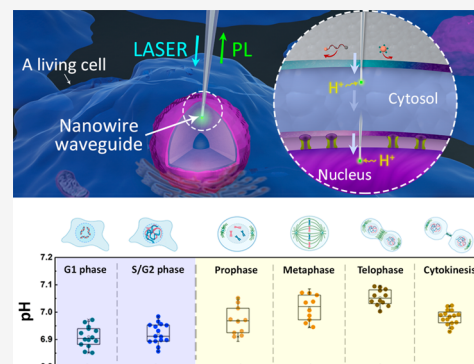
Cells are different from each other. Even in the same environments, genetically identical cells can display cell-to-cell variabilities, including cell morphology, proliferation, and growth and survival rates, as a result of individual compartmentalization of their own vital activities.[1] To understand the different behaviors of individual cells, it is significantly important to measure and analyze the variations in physiological parameters (e.g., pH, temperature, and oxygen levels) inside living cells.[2] In particular, subcellular compartments, such as the nucleus, mitochondria, and endoplasmic reticulum, perform distinct biological functions in a timely manner, so the variations should be monitored independently over time.[3,4] Specifically, due to different levels of cellular metabolism, there can be spatiotemporal pH heterogeneity;[5] theoretically, local pH has been predicted to fluctuate during cell division by successive catabolism or anabolism,[6,7] and when activated by apoptotic stimuli, programmed cell death leads to mitochondrial dysfunction, followed by abrupt acidification of the intracellular milieu.[8]

Due to the significance of local pH variations, there have been extensive studies in developing in situ monitoring systems capable of reporting subcellular pH in real time. A variety of pH-sensitive molecular probes (e.g., fluorescent dyes and quantum dots) are available for pH detection[9–11] that can be internalized into living cells by electroporation or thorough endocytosis across otherwise impermeable cell membranes.[12] However, due to the nature of spontaneous internalization, positioning the probes in desired locations, especially inside membrane-protected organelles, remains a technical challenge. Although

pH-responsive fluorescent proteins can be genetically encoded inside engineered cells, elaborate gene engineering relevant to their expression, and subsequent transportation by protein trafficking is extremely difficult.[13,14] As alternatives, nano-pipettes[15,16] or optical fibers[17] have been directly inserted into a target cell. However, without precise control of their size and shape, drilling a hole in the membrane is fatal to the cell. In addition, their pH detection could not be localized because the sensing regions were relatively too large ($10–20\ \mu m$) to detect pH in cellular compartments in single cells.[15–19] Indeed, there is an unmet technological need for real-time pH monitoring of cellular compartments across multiple impermeable membranes in a single living cell.

In this work, we fabricated a mechanically robust yet tolerably thin nanowire waveguide capable of monitoring pH dynamics in desired cellular compartments via direct optical communication. Our poly(vinylbenzyl azide) ($PVBN_3$) nanowire is structurally strong and long enough to penetrate cell and organelle membranes, while its narrow diameter ($\sim$200 nm) ensures negligible cell damage and leakage. Chemically labeled high-density fluorescein on the tip ($\leq$500 nm) of nanowire
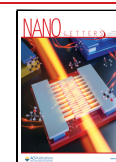
waveguide, which also enables for positional pH measurement in a given cellular compartment, can quickly respond to local pH variations, and through the nanowire waveguide, the pH-sensitive photoluminescence (PL) signals are directly transmitted to a spectrometer (<100 ms), minimizing optical loss and surrounding noise. Using the in situ pH detection system, we continuously monitored pH changes of different compartments inside a single living cell, allowing several scientific discoveries, such as organelle-exclusive pH homeostasis and stimuli-selective pH regulations. In particular, we demonstrated for the first time that during the cell cycle, the nucleus displays pH homeostasis in interphase but a tidal pH curve in the mitotic phase, newly implying the existence of independent pH-regulating activities by the nuclear envelope; this is attributed to the unique capability of our nanowire waveguide in the live streaming of subcellular events by local pH monitoring of a single living cell.

Design of a Real-Time Local pH-Reporting Nanowire Waveguide. By chemically labeling pH-responsive fluorescent dyes[20] on one end of polymeric nanowire, we successfully created a nanowire waveguide tailored for in situ monitoring of local pH over time in a single living cell (Figure 1a). In detail, by
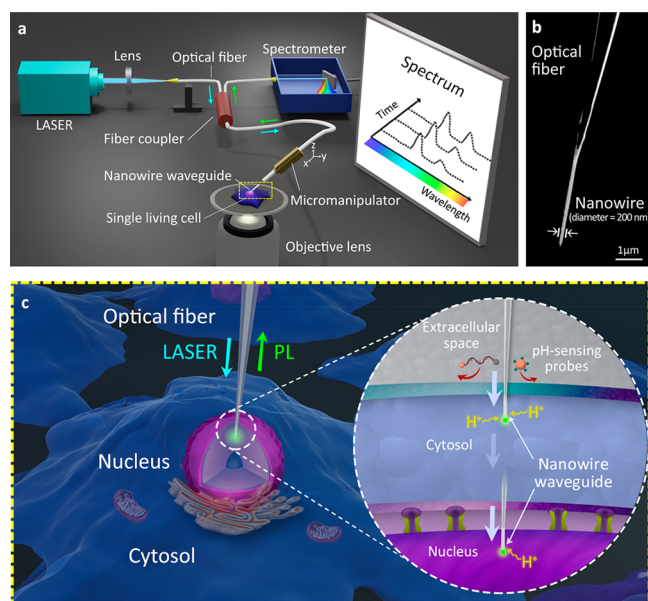

Figure 1. Design of a nanowire waveguide capable of reporting spatiotemporal pH changes within a single living cell. (a) Nanowire waveguide system for in situ pH monitoring in subcellular compartments in real time via direct optical communication. When a laser beam is transferred to the nanowire waveguide through the optical fiber and the fiber coupler (cyan arrow), the pH-sensitive fluorescein on the end of the nanowire emits a photoluminescent (PL) signal, which is directly transmitted to a spectrometer (green arrow) with no environmental interference in optical communication. Positioning the nanowire waveguide within a living cell can be precisely controlled by a three-axis micromanipulator (resolution: 0.5 μm) under observation by confocal fluorescence microscopy. (b) Field emission scanning electron microscopy image of our nanowire waveguide directly grown on the tip of a tapered optical fiber. Scale bar, 1 μm. (c) Local pH monitoring in a living cell across rigid cell and organelle membranes. As our long and thin nanowire waveguide is mechanically strong for leakage-free membrane penetration, its fluorescein-labeled terminal can be readily located at desired positions (in either the cytosol or the nucleus) for in situ pH detection (see inset). Depending on local proton concentrations, the intensity of the PL signal changes quickly, which can be monitored in real time through the nanowire waveguide.

evaporation of PVBN$_3$ solution (Figure S1), an elongated PVBN$_3$ nanowire was directly grown on the tip of a tapered optical fiber (Figure 1b and Figure S2), which was connected to a laser source and a spectrometer by an optical fiber coupler. As the surface of the nanowire was full of azide moieties ($-$N$_3$), its restricted exposure to dibenzocyclooctyne (DBCO)-functionalized fluorescein allowed the terminus of the nanowire ($\sim$500 nm in length) to be selectively modified with high-density pH reporters (0.117 $\pm$ 0.008 molecules$\cdot$nm^{-2}) via a copper-free click reaction (Figures S3 and S4). Importantly, our nanowire waveguide served as a great simultaneous *bidirectional* transmission path of the excitation laser (cyan arrow) and the PL signal (green arrow) from the localized fluorescein; as the PL signal was directly transmitted to the spectrometer, the intensity of the PL spectrum, which changed with proton concentration in a desired location, was measured in real time, regardless of the surroundings of the nanowire waveguide (Figure 1c).

The physical and optical characteristics of our nanowire waveguide were highly compatible for reporting the subcellular pH inside a living cell. Based on a previous study of nanowire dimensions minimizing cell damage,[21] we prepared a nanowire waveguide with a diameter of $\sim$200 nm (Figure 1b) and supersmooth surface (Figure S5), as precisely controlled by our confined-growth method.[22] Despite the small diameter, the high Young's modulus of PVBN$_3$ ($E \sim$ 1.7 GPa)[23] allowed the nanowire waveguide to readily penetrate a rigid matrix, whether conjugated with fluorescein or not (Figure S6). Importantly, the scattering loss at the junction was negligible (white dotted circles, Figure S7), mostly due to the directly and coaxially grown nanowire on the tip of the tapered optical fiber, resulting in strong propagation of injected LASER light to the tip of the nanowire (yellow dotted circles, Figure S7). Furthermore, we quantitatively measured the coupling efficiency at the junction by comparing the power at the tip of a nanowire waveguide (green symbols, PNW) and at the tip of a tapered optical fiber (blue symbols, POF) in Figure S8. Remarkably, the coupling efficiency (red symbols) was very high as 94.4 $\pm$ 1.6% even in various LASER powers. Moreover, the high refractive index of PVBN$_3$ ($n \sim$ 1.67),[24] compared with that of cellular environments ($n \sim$ 1.37),[25] permitted efficient transmission of light through the nanowire in cellular environments.

Optical Response of the Nanowire Waveguide to Local pH Variations. Using our microphotoluminescence setup (Figure 1a), we investigated the pH response of the nanowire waveguide in solutions with varying pH values (4$-$8) (Figure 2a). When the nanowire waveguide was dipped in different pH droplets, pH-dependent PL spectra were successfully obtained upon laser excitation (λ = 473 nm); the PL peak intensities at 535 nm (I_{535}) showed a gradual increment with increasing pH, consistent with the well-known pH-dependent characteristic of fluorescein.[20] As the intensities at 685 nm (I_{685}) exhibited negligible variations with increasing pH, they served as reference signals for the remainder of pH monitoring. We verified the consistency of pH variations among different nanowire waveguides, as demonstrated in Figure S9a. Importantly, the nanowire waveguides exhibited excellent photostability up to 60 s under continuous laser exposure (Figure S9b), and cyclic variations in pH between 5.0 and 7.5 were reproducible (Figure S9c).

The PL spectra through the nanowire waveguides responded to pH changes within very short times (<100 ms) (Figure 2 and Figure S10). Here, the integration time of the PL signals was taken to be 50 ms (the temporal resolution of the pH sensing, as
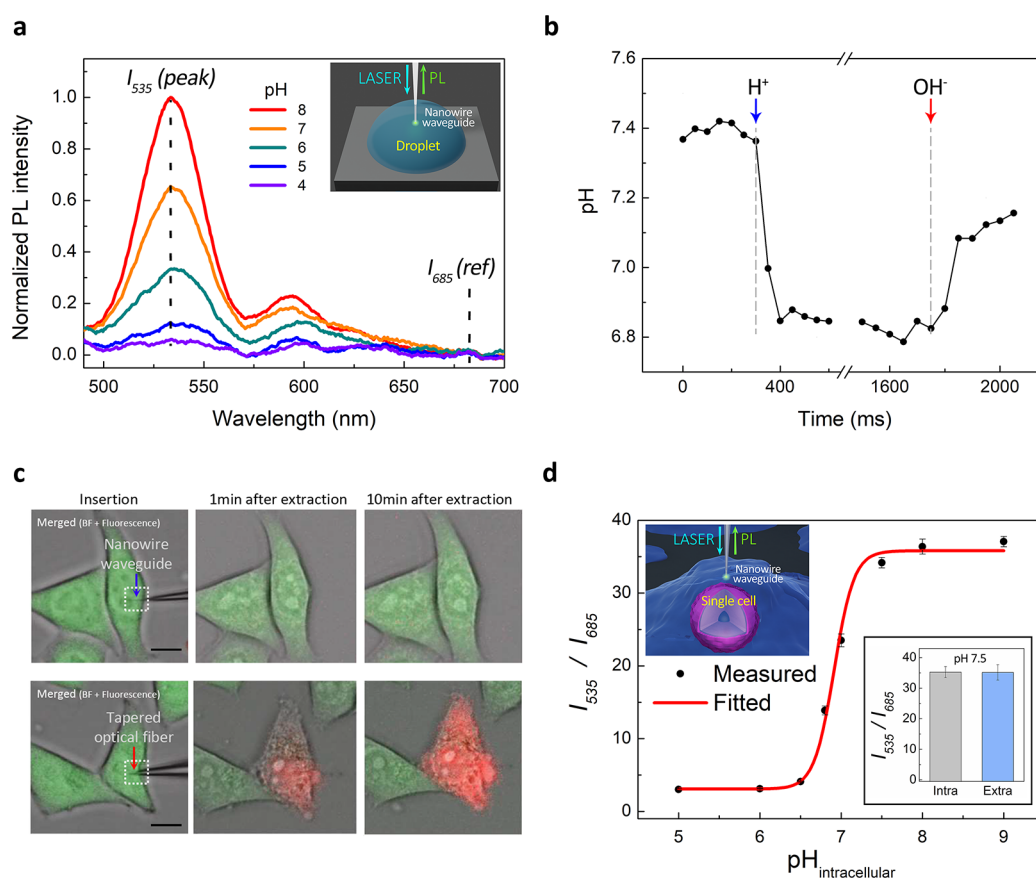
Figure 2. Characterization of our nanowire waveguide to be used for sensitive and rapid pH reporting in a cellular environment with negligible cell damage. (a) When varying pH from 4 to 8 for a droplet (see inset), the dipped nanowire waveguide successfully reported pH-dependent PL spectra upon laser excitation ($\lambda = 473$ nm). (b) Time-dependent fluorescent signals ($\lambda = 535$ nm) were monitored in real time by the nanowire waveguide due to the quick response to pH changes (<100 ms). Blue and red arrows indicate injection points of acidic and basic solutions, respectively. (c) Nanowire waveguide (blue arrow; diameter ~200 nm) could be readily inserted into living cells (top), whereas a tapered optical fiber (red arrow; tip diameter ~200 nm) caused severe cell damage and leakage (bottom). For the live or dead cell viability assay, the HeLa cells were stained with calcein-AM (green) and propidium iodide (red). Scale bar, 10 μm. (d) A pH calibration curve (red) was obtained by measuring the normalized PL peak intensities (I_{535}/I_{685}) in nigericin-treated cells in the pH range of 5−9 ($n = 3$), which was followed by fitting with a Boltzmann function ($R^2 = 0.9969$). As measured in the HeLa cells treated with nigericin at pH 7.5 ($n = 3$), the normalized PL peak intensities inside (gray) and outside (blue) the cells were equalized, indicating that intracellular and extracellular pH values were the same (inset).

determined in Figure S11). For instance, when the initially nanowire-dipped droplet with a pH of 7.5 was rapidly acidified to pH 6.8 (Figure 2b, blue arrow), the PL peak intensity sharply decreased in less than 100 ms to reach the signal corresponding to the correct pH. Conversely, when the slightly acidic droplet was mixed with a basic buffer solution, the PL peak intensity sharply increased, indicating that the final pH was 7.2 (Figure 2b, red arrow). It is well-known that as fluorescein reacts instantaneously with H^{+},[20] the rate-determining step of the pH-responsive behavior would be proton diffusion in the droplet. Considering that the proton diffusion rate in intracellular fluids is not significantly different from that in buffer solution,[26] the quick fluorescent response to pH changes implies that our nanowire waveguide would be capable of monitoring pH changes in real-time even in intracellular environments.

Applicability of the Nanowire Waveguide for pH Monitoring inside Living Cells. Deep injection of our nanowire waveguide did not cause living cells to be severely damaged (Figure 2c and Movie S1). For real-time observation of cell viability, HeLa cells were stained with calcein-AM and propidium iodide (PI), which emit green and red fluorescence in live and dead cells, respectively. As attributed to the fine

diameter (~200 nm) and uniformly stretched structure of the PVBN₃ nanowire, our nanowire waveguide caused negligible damage to the cells from its insertion through 10 min after extraction (Figure 2c, top panel). Importantly, evidenced by the lack of a red fluorescence signal, we found that the PI dye did not enter the intracellular space during the nanowire waveguide insertion or after extraction, confirming that membrane integrity was well preserved (Figure S12). Moreover, the cell morphology was obviously unaffected even after extraction, implying that our in situ pH monitoring system is free of membrane rupture and deformation.

Conversely, the insertion of a tapered optical fiber with a typical conical shape instantly led to cell death, as membrane rupture was observed with intracellular fluid leakage at the point of insertion (Figure 2c, bottom panel, and Figure S12). When we compared cell viability by inserting the nanowire waveguide and the tapered optical fiber into the cytosol and nuclei of HeLa cells, our nanowire waveguide showed definitely higher cell viability (100% in the cytosol and the nuclei) than the tapered optical fiber (33% in the cytosol; 25% in the nuclei) (Figure S13). We note that the cell viability by our nanowire waveguide strategy is
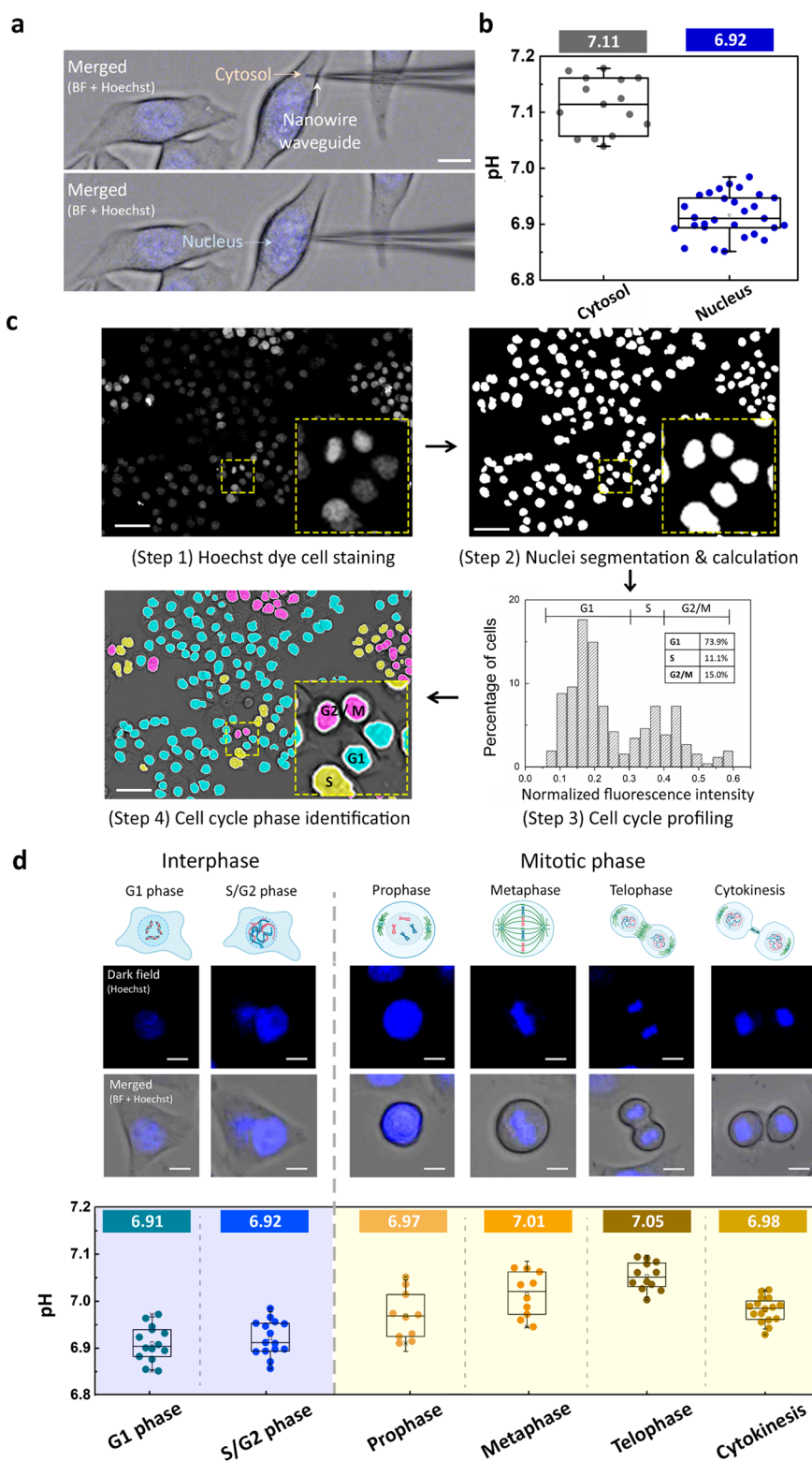
Figure 3. In situ pH monitoring in different compartments during a cell cycle. (a) Nanowire waveguide was inserted into the cytosol (top) and nuclei (bottom) of living HeLa cells that were stained with Hoechst dyes. Scale bar, 10 μm. (b) Comparison between cytosolic pH ($n = 15$) and nuclear pH ($n = 29$). (c) Identification of cell cycle stages for individual HeLa cells. When Hoechst dyes specifically stained nuclei of living cells (step 1), the net fluorescence intensities of the nuclei were calculated for all the cells using our automated image segmentation algorithm (step 2), and a DNA histogram was prepared to profile the cell cycles of HeLa cells (step 3). By color mapping on the cell image, we identified the phase of each cell (step 4). Scale bar, 50 μm. (d) Nuclear pH measured for each cell cycle phase. Schematics of cell cycle phases (top), dark field and merged (bright field + fluorescence) images of Hoechst-stained cells (middle), and nuclear pH values (bottom) are displayed for different cell cycle phases. G1 and S/G2 phases showed similar pH values (G1 phase: 6.91 ± 0.03 ($n = 14$); S/G2 phase: 6.92 ± 0.03 ($n = 15$)), while the nuclear pH values in prophase, metaphase, telophase, and cytokinesis exhibited a tidal curve (prophase: 6.97 ± 0.05 ($n = 10$); metaphase: 7.01 ± 0.05 ($n = 10$); telophase: 7.05 ± 0.03 ($n = 12$); cytokinesis: 6.98 ± 0.03 ($n = 16$)). Scale bar, 10 μm.
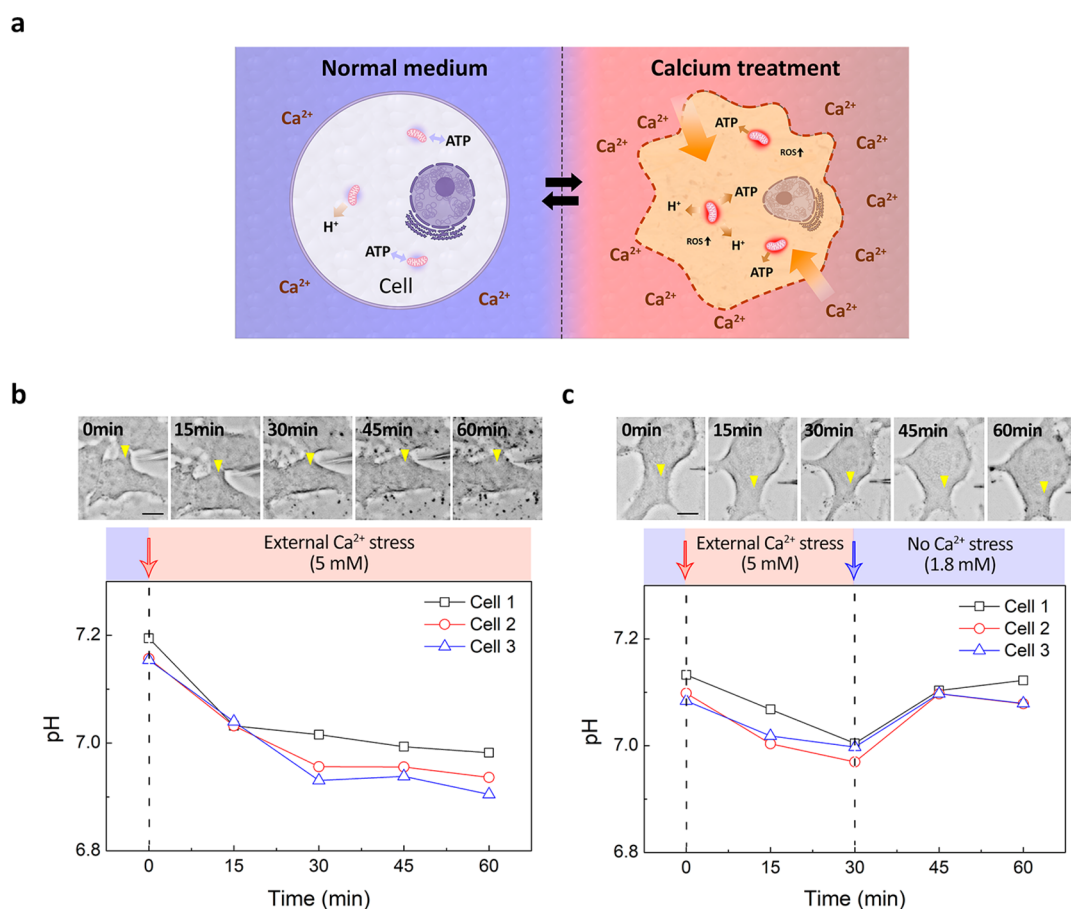
Figure 4. Cytosolic pH variations in response to external calcium ions. (a) Schematic illustration of intracellular acidification in the presence of excessive calcium ions. In general, high concentrations of calcium ions elicit adverse effects on cells, including overproduction of adenosine triphosphates (ATPs) and reactive oxygen species (ROS), thereby affecting pH homeostasis. (b,c) Different cellular responses against external calcium ion stresses were reported by different cytosolic pH variations ($n = 3$). Yellow triangles in bright-field images indicate where our nanowire waveguide was inserted for pH measurements. Red and blue arrows indicate introduction and removal points of external Ca^{2+} stress (5 mM), respectively. Scale bar, 10 μm.

higher than those of other types of strategies with carriers for biosensing probes (Table S1).

We validated that pH monitoring through our nanowire waveguide ensures high accuracy even in the presence of complex cellular components (Figure 2d). To systematically manipulate the intracellular pH, HeLa cells were incubated in buffer solutions with different pH values (5–9), including the K^+/H^+-ionophore nigericin.[27] By measuring the intensity ratio (I_{535}/I_{685}) of nigericin-treated HeLa cells at fixed pH, we successfully obtained a pH calibration curve for intracellular pH monitoring (red line in Figure 2d and Figure S14). From this curve, we confirmed that the detectable range (pH 6.5–7.5) of our nanowire waveguide is perfectly suitable for reporting the pH of living cells.[3] Interestingly, our nanowire waveguide always yielded almost the same signals, irrespective of its surroundings, as demonstrated at pH 7.5 (the right inset in Figure 2d and Figure S15a,b,d) and in other experimental groups (Figure S15c,e). From this observation, it was concluded that our nanowire waveguide can respond to pH variations accurately, even in complex cellular environments.[28]

Organelle-Exclusive pH Monitoring during a Cell Cycle. As our nanowire waveguide is able to exclusively monitor the local pH of different compartments in real time, we demonstrated in situ monitoring of dynamic pH patterns for the cytosol and nuclei within single living cells (Figure 3a,b and

Movie S2). Despite the importance of the nuclear pH in regulating critical cellular functions (e.g., DNA replication, gene expression, and epigenetic modulation),[29,30] direct determination of the internal pH has been extremely difficult,[31] which is mostly because of the presence of two robust compartmentalizing membranes: the cellular membrane and the nuclear envelope. Due to large-diameter (~120 nm) nuclear pores within the nuclear envelope, a number of studies have assumed that the pH in the nucleus is identical to that in the cytosol.[32,33] However, based on recent efforts over the past decade, it was suggested that the nuclear compartment can control its own internal pH, thereby making the nuclear pH differ from the cytosolic pH.[33–35] To answer this controversial question, we separately measured the pH of the nucleus and the cytosol by inserting the nanowire waveguide into the desired sites of single living HeLa cells (Figure 3a). The insertion of the nanowire waveguide into the nuclear space was verified by pH measurements while varying the x, y, and z coordinates of the nanowire waveguide tip (Figures S16 and S17). As a result, we found that the nuclear pH (6.92 ± 0.04, $n = 29$) was meaningfully lower than the cytosolic pH (7.11 ± 0.05, $n = 15$) (Figure 3b), implying that there could be a pH gradient between the nucleus and the cytosol by separate pH regulations. We note that the distance from the nanowire-inserted plasma membrane to the nuclear one in cytosol did not affect positional

pH measurements (Figure S18). In addition, the insertion of the nanowires did not cause fluorescent signal changes in the living cells, indicating no stress response by its insertion. In contrast, the significant stress response was observed by the insertion of the tapered optical fiber (Movie S3). Here, we observed no deformation or buckling of the nanowire waveguide even after 20 times of its insertion into the cytosol of living HeLa cells (Figure S19), due to its geometry and superior mechanical property (Figure S20 and Movie S4).

As the robust membrane of the nucleus was easily penetrated by our nanowire waveguide with no leakage, we directly monitored nuclear pH variations throughout the entire human cell cycle (Figure 3c,d). Preliminarily, it was necessary to identify the cell cycle status of individual HeLa cells;[36] in principle, as cell division progresses, the total DNA quantity inside the nucleus varies, which can be quantified to determine the cell cycle stage of dividing cells. In detail, we stained the cells with Hoechst dye, which emits a fluorescent signal by specifically binding to DNAs inside the nuclei, and the DNA content of each cell was measured by automated algorithm, in which the total fluorescence intensities were calculated for a number of nuclei. Finally, the phase of each cell was identified based on the DNA histogram, as demonstrated by color mapping on the cell image. From the analysis, we ascertained the cell cycle phase (G1, S, and G2/M) of individual HeLa cells and subsequently obtained the ratio of each phase, which was well matched to the reported characteristics of HeLa cells (G1, 72.1%; S, 12.6%; G2/M, 12%).[37]

Based on the assessment of each cell cycle stage, we then measured nuclear pH variations during cell division, discovering pH homeostasis in interphase and pH fluctuation in the mitotic phase (Figure 3d). Specifically, the HeLa cells in the G1 and S/G2 phases exhibited similar pH values (G1 phase: 6.91 ± 0.03 ($n = 14$); S/G2 phase: 6.92 ± 0.03 ($n = 15$), Figure 3d, blue box). Previously, it was reported by several studies that during the interphase, the cytosol displayed pH fluctuations for several reasons, such as ATP synthesis/hydrolysis and redox oscillations.[6,38] However, we clearly observed that the nucleus preserved its own pH in G1 and S/G2 phases, presumably validating the maintenance of pH-regulating activities in the nuclear envelope; this nuclear pH homeostasis in the interphase is consistent with the previous finding for the nuclear pH variations of budding yeast.[39] Strikingly, when the HeLa cells entered prophase, the nuclear pH continued to slightly increase until the cells reached telophase (prophase: 6.97 ± 0.05 ($n = 10$); metaphase: 7.01 ± 0.05 ($n = 10$); telophase: 7.05 ± 0.03 ($n = 12$), Figure 3d, yellow box, and Figures S21 and S22). During the mitotic phase, the transient disruption of nuclear pH homeostasis might be related to the breakdown of the nuclear envelope,[40] temporarily interrupting the pH regulation abilities of the nucleus. However, as the cells arrived at a cytokinesis phase at the end of mitosis, the nuclear pH returned to its original pH value (cytokinesis: 6.98 ± 0.03 ($n = 16$)). A different type of cells (MCF-7 cell) also exhibited similar pH behavior to HeLa cells during mitotic phase (prophase: 7.06 ± 0.02 ($n = 7$); metaphase: 7.08 ± 0.03 ($n = 5$); telophase: 7.14 ± 0.03 ($n = 7$); cytokinesis: 7.08 ± 0.02 ($n = 6$), Figures S23 and S24). This result suggested that the reconstruction of divided cell nuclear envelopes would lead to the recovery of original pH homeostasis. By direct pH monitoring during the entire cell cycle, it was evident that the nucleus serves its own pH-regulating function.

Real-Time Cytosolic pH Monitoring in Response to Ionic Stress. Additionally, we investigated the cytosolic pH

dynamics of single living HeLa cells by providing external ion stresses, and it was confirmed that single cells indeed react differently in response to different ions (Figure 4). When excessive amounts of Ca^{2+} were added to the cell culture medium, the cytosolic pH decreased significantly (7.17 ± 0.02 to 6.97 ± 0.04) within 30 min as a result of intracellular acidification induced by high extracellular Ca^{2+} (Figure 4b). Interestingly, when Ca^{2+} was substituted with Mg^{2+}, there were negligible pH variations (7.09 ± 0.01 to 7.08 ± 0.01) (Figure S25). It is known that the presence of excess Ca^{2+} in extracellular medium can elicit the generation of reactive oxygen species (ROS), mitochondrial dysfunction by increasing ATP levels, as confirmed by the intracellular ATP assay (Figure S26).[41,42] Accordingly, it was considered that the intracellular acidification of HeLa cells occurred by the adverse effects of the high extracellular Ca^{2+}, which was further supported by scrutinizing cell viabilities depending on calcium ion treatments (Figure S27a). Moreover, our magnesium treatment experiment revealed that the cells were tolerant to the increase in extracellular Mg^{2+} concentrations; consistent with a previous report,[43] there were no cellular malfunctions or cell deaths (Figures S25 and S27b).

Importantly, living HeLa cells restored their original pH when the external ion stress was removed (Figure 4c). To observe the recovery in pH homeostasis, we incubated HeLa cells with excess amounts of Ca^{2+} for 30 min and then quickly adjusted the Ca^{2+} concentration of the medium to the normal range (1.8 mM) to monitor cytosolic pH variations in three individual cells. As observed from the previous Ca^{2+}-dependent intracellular acidification (Figure 4b), for the first 30 min, high extracellular Ca^{2+} induced the cytosol of HeLa cells to be acidic (7.10 ± 0.02 to 6.99 ± 0.02). Surprisingly, after the removal of extracellular Ca^{2+} stress (Figure 4c, blue arrow), the cells gradually restored their intrinsic pH (6.99 ± 0.02 to 7.09 ± 0.02), meaning that the cytosolic pH homeostasis of living HeLa cells was successfully recovered from the loss of pH control. It was interesting that the overall tendencies of HeLa cells against external ion stresses were similar, but their individual responses, as expressed in pH, were heterogeneous, probably related to cell-to-cell differences, such as size, morphology, and dividing phases.[44]

By exploiting the well-defined local pH-reporting nanowire waveguide, we successfully accessed different compartments without causing cell damage to monitor their pH dynamics in a single living cell. Across otherwise impenetrable plasma membranes and nuclear envelopes, our in situ pH monitoring is significant in that it can provide a fundamental understanding of the role of subcellular compartments. From the observation of the pH difference between the cytosol and the nucleus, it was confirmed again that differentiated cellular activities can be provided by compartmentalization, exhibiting different pH regulations.[33−35] In particular, pH homeostasis and fluctuation for cellular growth and division in the nucleus infer that, before breakdown, the nuclear envelope is involved in pH maintenance, as well as nuclear transport, in facilitating biosynthetic activities of the cell;[40,45] to the best of our knowledge, this is the first direct evidence of independent pH-regulating activities in the nucleus, specifically in dividing mammalian cells.

As observed by different cellular responses to external ionic stimuli, our local pH-monitoring nanowire waveguide would be widely applicable for studying an individual cell's life under diverse conditions. For instance, real-time detection of organelle-exclusive pH variations during various cellular behaviors (e.g., differentiation, cell signaling, and programmed

cell death) would be readily achievable to understand biological processes of different compartments.[3,4] Moreover, via highly efficient copper-free click chemistry, our PVBN$_3$ nanowire waveguide allows its specific surface area to be readily modified with other types of biosensing molecules (e.g., molecular beacons, monoclonal antibodies, and nucleic acid aptamers);[46] rather than pH variations, concentration dynamics for intracellular targets, such as mRNAs, or metabolites, would be readily monitored in a parallel manner. Given smaller diameter of the nanowire waveguide (down to ∼100 nm)[47] and the higher spatial resolution of the manipulator (down to ∼25 nm)[48] in combination with super-resolution microscopy, our in situ monitoring platform could be further advanced to cover many other membrane-enclosed small organelles, including endosomes and mitochondria, enabling us to obtain comprehensive information on a single living cell.

■ ASSOCIATED CONTENT

ⓈⒾ Supporting Information

The Supporting Information is available free of charge at https://pubs.acs.org/doi/10.1021/acs.nanolett.2c02185.

> Experimental section, materials and methods, characterization of pH-monitoring nanowire waveguide with Nuclear Magnetic Resonance(NMR), Transmission Electron Microscope(TEM), Optical Microscope (OM), and spectrometry, local pH monitoring by the nanowire waveguide during a cell cycle (PDF)

> Movie S1: Cell viability comparison between the insertions of a nanowire waveguide and a tapered optical fiber into living HeLa cells (MP4)

> Movie S2: Demonstration of real-time pH measurement using the nanowire waveguide in a single living HeLa cell (MP4)

> Movie S3: Stress response comparison between the insertions of a nanowire waveguide and a tapered optical fiber into living HeLa cells (MP4)

> Movie S4: Demonstration of inserting the nanowire waveguide into a living HeLa cell (MP4)

■ AUTHOR INFORMATION

Corresponding Authors

Seung Soo Oh − *Department of Materials Science and Engineering, Pohang University of Science and Technology (POSTECH), Pohang, Gyeongbuk 37673, South Korea;* ⓞ orcid.org/0000-0001-8045-080X; Email: seungsoo@postech.ac.kr

Jung Ho Je − *X-ray Imaging Center and Department of Materials Science and Engineering, Pohang University of Science and Technology (POSTECH), Pohang, Gyeongbuk 37673, South Korea;* ⓞ orcid.org/0000-0001-8862-0260; Email: jhje@postech.ac.kr

Authors

Moon-Jung Yong − *X-ray Imaging Center and Department of Materials Science and Engineering, Pohang University of Science and Technology (POSTECH), Pohang, Gyeongbuk 37673, South Korea*

Byunghwa Kang − *Department of Materials Science and Engineering, Pohang University of Science and Technology (POSTECH), Pohang, Gyeongbuk 37673, South Korea*

Un Yang − *X-ray Imaging Center and Department of Materials Science and Engineering, Pohang University of Science and*

Technology (POSTECH), Pohang, Gyeongbuk 37673, South Korea

Complete contact information is available at:
https://pubs.acs.org/10.1021/acs.nanolett.2c02185

Author Contributions

S.S.O. and J.H.J. conceived the study and designed the experiments. M.-J.Y. conducted the experiments and analyzed the data. B.K. performed the various cell preparation and contributed to the intracellular pH measurement experiments. U.Y. developed the cell identification model and performed the data processing. S.S.O. and J.H.J. supervised the research. All the authors discussed the results and wrote the manuscript. M.-J.Y., B.K., and U.Y. contributed equally to this work.

Notes

The authors declare no competing financial interest.

■ REFERENCES

(1) Stoeger, T.; Battich, N.; Pelkmans, L. Passive Noise Filtering by Cellular Compartmentalization. *Cell* **2016**, *164*, 1151−1161.

(2) Zhang, X.-a.; Zhang, W.; Wang, Q.; Wang, J.; Ren, G.; Wang, X.-d. Quadruply-Labeled Serum Albumin as a Biodegradable Nanosensor for Simultaneous Fluorescence Imaging of Intracellular PH Values, Oxygen and Temperature. *Microchim. Acta* **2019**, *186*, 584−595.

(3) Jaworska, A.; Malek, K.; Kudelski, A. Intracellular PH − Advantages and Pitfalls of Surface-Enhanced Raman Scattering and Fluorescence Microscopy − A Review. *Spectrochim. Acta - Part A Mol. Biomol. Spectrosc.* **2021**, *251*, 119410.

(4) Han, J.; Burgess, K. Fluorescent Indicators for Intracellular PH. *Chem. Rev.* **2010**, *110*, 2709−2728.

(5) Søndergaard, R. V.; Henriksen, J. R.; Andresen, T. L. Design, Calibration and Application of Broad-Range Optical Nanosensors for Determining Intracellular PH. *Nat. Protoc.* **2014**, *9*, 2841−2858.

(6) Da Veiga Moreira, J.; Peres, S.; Steyaert, J. M.; Bigan, E.; Paulevé, L.; Nogueira, M. L.; Schwartz, L. Cell Cycle Progression Is Regulated by Intertwined Redox Oscillators. *Theor. Biol. Med. Model.* **2015**, *12*, 10.

(7) Gagliardi, L. J.; Shain, D. H. Is Intracellular PH a Clock for Mitosis? *Theor. Biol. Med. Model.* **2013**, *10*, 10.

(8) Matsuyama, S.; Llopis, J.; Deveraux, Q. L.; Tsien, R. Y.; Reed, J. C. Changes in Intramitochondrial and Cytosolic PH: Early Events That Modulate Caspase Activation during Apoptosis. *Nat. Cell Biol.* **2000**, *2*, 318−325.

(9) He, C.; Lu, K.; Lin, W. Nanoscale Metal-Organic Frameworks for Real-Time Intracellular PH Sensing in Live Cells. *J. Am. Chem. Soc.* **2014**, *136*, 12253−12256.

(10) Dennis, A. M.; Rhee, W. J.; Sotto, D.; Dublin, S. N.; Bao, G. Quantum Dot-Fluorescent Protein Fret Probes for Sensing Intracellular PH. *ACS Nano* **2012**, *6*, 2917−2924.

(11) Shen, Y.; Liang, L.; Zhang, S.; Huang, D.; Zhang, J.; Xu, S.; Liang, C.; Xu, W. Organelle-Targeting Surface-Enhanced Raman Scattering (SERS) Nanosensors for Subcellular PH Sensing. *Nanoscale* **2018**, *10*, 1622−1630.

(12) Albertazzi, L.; Storti, B.; Marchetti, L.; Beltram, F. Delivery and Subcellular Targeting of Dendrimer-Based Fluorescent PH Sensors in Living Cells. *J. Am. Chem. Soc.* **2010**, *132*, 18158−18167.

(13) Kneen, M.; Farinas, J.; Li, Y.; Verkman, A. S. Green Fluorescent Protein as a Noninvasive Intracellular PH Indicator. *Biophys. J.* **1998**, *74*, 1591−1599.

(14) Palmer, A. E.; Qin, Y.; Park, J. G.; McCombs, J. E. Design and Application of Genetically Encoded Biosensors. *Trends Biotechnol.* **2011**, *29*, 144−152.

(15) Zhang, Y.; Clausmeyer, J.; Babakinejad, B.; López Córdoba, A.; Ali, T.; Shevchuk, A.; Takahashi, Y.; Novak, P.; Edwards, C.; Lab, M.; Gopal, S.; Chiappini, C.; Anand, U.; Magnani, L.; Coombes, R. C.; Gorelik, J.; Matsue, T.; Schuhmann, W.; Klenerman, D.; Sviderskaya, E. V.; Korchev, Y. Spearhead Nanometric Field-Effect Transistor Sensors for Single-Cell Analysis. *ACS Nano* **2016**, *10*, 3214−3221.

(16) Guo, J.; Sesena Rubfiaro, A.; Lai, Y.; Moscoso, J.; Chen, F.; Liu, Y.; Wang, X.; He, J. D Ynamic Single-Cell Intracellular PH Sensing Using a SERS-Active Nanopipette. *Analyst* **2020**, *145*, 4852−4859.

(17) Yang, Q.; Zhang, X.; Song, Y.; Li, K.; Shi, H.; Xiao, H.; Ma, Y. Label-free in Situ PH Monitoring in a Single Living Cell Using an Optical Nanoprobe. *Med. Devices Sensors* **2020**, *3*, e10079.

(18) Vo-Dinh, T.; Alarie, J. P.; Cullum, B. M.; Griffin, G. D. Antibody-Based Nanoprobe for Measurement of a Fluorescent Analyte in a Single Cell. *Nat. Biotechnol.* **2000**, *18*, 764−767.

(19) Scaffidi, J. P.; Gregas, M. K.; Seewaldt, V.; Vo-Dinh, T. SERS-Based Plasmonic Nanobiosensing in Single Living Cells. *Anal. Bioanal. Chem.* **2009**, *393*, 1135−1141.

(20) Alvarez-Pez, J. M.; Ballesteros, L.; Talavera, E.; Yguerabide, J. Fluorescein Excited-State Proton Exchange Reactions: Nanosecond Emission Kinetics and Correlation with Steady-State Fluorescence Intensity. *J. Phys. Chem. A* **2001**, *105*, 6320−6332.

(21) Obataya, I.; Nakamura, C.; Han, S. W.; Nakamura, N.; Miyake, J. Direct Insertion of Proteins into a Living Cell Using an Atomic Force Microscope with a Nanoneedle. *Nanobiotechnology* **2005**, *1*, 347−352.

(22) Je, J. H.; Yang, U.; Oh, S. S.; Yong, M. J.; Kang, B. H. Method of forming micro-or nanowires at predetermined positions of an object using a micro- or nanopipette. U.S. Patent Appl. US17,306,220, 2021.

(23) Bicerano, J. *Prediction of Polymer Properties*, 2nd ed.; Marcel Dekker: New York, 1996.

(24) Zaniboni, M.; Swietach, P.; Rossini, A.; Yamamoto, T.; Spitzer, K. W.; Vaughan-Jones, R. D. Intracellular Proton Mobility and Buffering Power in Cardiac Ventricular Myocytes from Rat, Rabbit, and Guinea Pig. *Am. J. Physiol. - Heart Circ. Physiol.* **2003**, *285*, 1236−1246.

(25) James, J.; Hanna, J. M.; Subila, K. B. Refractive Index Engineering using Polymer Nanocomposites. PhD thesis, University of South Brittany, France, 2019.

(26) Liu, P. Y.; Chin, L. K.; Ser, W.; Chen, H. F.; Hsieh, C. M.; Lee, C. H.; Sung, K. B.; Ayi, T. C.; Yap, P. H.; Liedberg, B.; Wang, K.; Bourouina, T.; Leprince-Wang, Y. Cell Refractive Index for Cell Biology and Disease Diagnosis: Past, Present and Future. *Lab Chip* **2016**, *16*, 634−644.

(27) Llopis, J.; McCaffery, J. M.; Miyawaki, A.; Farquhar, M. G.; Tsien, R. Y. Measurement of Cytosolic, Mitochondrial, and Golgi PH in Single Living Cells with Green Fluorescent Proteins. *Proc. Natl. Acad. Sci. U. S. A.* **1998**, *95*, 6803−6808.

(28) Ellis, R. J. Macromolecular Crowding: An Important but Neglected Aspect of the Intracellular Environment. *Curr. Opin. Struct. Biol.* **2001**, *11*, 114−119.

(29) Francastel, C.; Schübeler, D.; Martin, D. I. K.; Groudine, M. Nuclear Compartmentalization and Gene Activity. *Nat. Rev. Mol. Cell Biol.* **2000**, *1*, 137−143.

(30) Nakamura, A.; Tsukiji, S. Ratiometric Fluorescence Imaging of Nuclear PH in Living Cells Using Hoechst-Tagged Fluorescein. *Bioorg. Med. Chem. Lett.* **2017**, *27*, 3127−3130.

(31) Casey, J. R.; Grinstein, S.; Orlowski, J. Sensors and Regulators of Intracellular PH. *Nat. Rev. Mol. Cell Biol.* **2010**, *11*, 50−61.

(32) Fabre, E.; Hurt, E. C. Nuclear Transport. *Curr. Opin. Cell Biol.* **1994**, *6*, 335−342.

(33) Sherman, T. A.; Rongali, S. C.; Matthews, T. A.; Pfeiffer, J.; Nehrke, K. Identification of a Nuclear Carbonic Anhydrase in Caenorhabditis Elegans. *Biochim. Biophys. Acta - Mol. Cell Res.* **2012**, *1823*, 808−817.

(34) Santos, J. M.; Martínez-Zaguilán, R.; Facanha, A. R.; Hussain, F.; Sennoune, S. R. Vacuolar H+-ATPase in the Nuclear Membranes Regulates Nucleo-Cytosolic Proton Gradients. *Am. J. Physiol. - Cell Physiol.* **2016**, *311*, C547−C558.

(35) Seksek, O.; Bolard, J. Nuclear PH Gradient in Mammalian Cells Revealed by Laser Microspectrofluorimetry. *J. Cell Sci.* **1996**, *109*, 257−262.

(36) Roukos, V.; Pegoraro, G.; Voss, T. C.; Misteli, T. Cell Cycle Staging of Individual Cells by Fluorescence Microscopy. *Nat. Protoc.* **2015**, *10*, 334−348.

(37) Athukorala, Y.; Trang, S.; Kwok, C.; Yuan, Y. V. Antiproliferative and Antioxidant Activities and Mycosporine-Like Amino Acid Profiles of Wild-Harvested and Cultivated Edible Canadian Marine Red Macroalgae. *Molecules* **2016**, *21*, 119.

(38) DeBerardinis, R. J.; Lum, J. J.; Hatzivassiliou, G.; Thompson, C. B. The Biology of Cancer: Metabolic Reprogramming Fuels Cell Growth and Proliferation. *Cell Metab.* **2008**, *7*, 11−20.

(39) Zhao, H.; Zhang, Y.; Pan, M.; Song, Y.; Bai, L.; Miao, Y.; Huang, Y.; Zhu, X.; Song, C. P. Dynamic Imaging of Cellular PH and Redox Homeostasis with a Genetically Encoded Dual-Functional Biosensor, PHaROS, in Yeast. *J. Biol. Chem.* **2019**, *294*, 15768−15780.

(40) Cooper, G. M. *The Cell: A Molecular Approach*, 2nd ed.; Sinauer Associates: Sunderland, MA, 2000.

(41) McGinnis, K. M.; Wang, K. K. W.; Gnegy, M. E. Alterations of Extracellular Calcium Elicit Selective Modes of Cell Death and Protease Activation in SH-SY5Y Human Neuroblastoma Cells. *J. Neurochem.* **1999**, *72*, 1853−1863.

(42) Voccoli, V.; Tonazzini, I.; Signore, G.; Caleo, M.; Cecchini, M. Role of Extracellular Calcium and Mitochondrial Oxygen Species in Psychosine-Induced Oligodendrocyte Cell Death. *Cell Death Dis.* **2014**, *5*, e1529.

(43) Libako, P.; Castiglioni, S.; Baldoli, E.; Mazur, A.; Nowacki, W.; Maier, J. A. M. Blocking the Rise of Intracellular Calcium Inhibits the Growth of Cells Cultured in Different Concentrations of Magnesium. *Magnes. Res.* **2012**, *25*, 12−20.

(44) Kültz, D. Molecular and Evolutionary Basis of the Cellular Stress Response. *Annu. Rev. Physiol.* **2005**, *67*, 225−257.

(45) Demaurex, N. pH Homeostasis of Cellular Organelles. *News Physiol. Sci.* **2002**, *17*, 1−5.

(46) Bidar, N.; Amini, M.; Oroojalian, F.; Baradaran, B.; Hosseini, S. S.; Shahbazi, M. A.; Hashemzaei, M.; Mokhtarzadeh, A.; Hamblin, M. R.; de la Guardia, M. Molecular Beacon Strategies for Sensing Purpose. *TrAC - Trends Anal. Chem.* **2021**, *134*, 116143.

(47) Kim, J. T.; Seol, S. K.; Pyo, J.; Lee, J. S.; Je, J. H.; Margaritondo, G. Three-Dimensional Writing of Conducting Polymer Nanowire Arrays by Meniscus-Guided Polymerization. *Adv. Mater.* **2011**, *23*, 1968−1970.

(48) Watanabe, K.; Yokote, H. A Microstep Controller of a DC Servomotor. *IEEE Trans. Instrum. Meas.* **1990**, *39*, 867−869.